

1 **Polar record of Early Jurassic massive carbon injection**

2

3 Guillaume Suan^{1,2}†, Boris L. Nikitenko³, Mikhail A. Rogov⁴, François Baudin⁵, Jorge E.
4 Spangenberg⁶, Valeriy G. Knyazev⁷, Larisa A. Glinskikh³, Anna A. Goryacheva³, Thierry
5 Adatte¹, James B. Riding⁸, Karl B. Föllmi¹, Bernard Pittet², Emanuela Mattioli², and
6 Christophe Lécuyer^{2,9}

7

8 ¹Institut de Géologie et de Paléontologie, Université de Lausanne, Anthropole, CH-1015
9 Lausanne, Switzerland

10 ²UMR CNRS 5276 LGLTPE, Université Lyon 1, Campus de la Doua, Bâtiment Géode, F-
11 69622 Villeurbanne Cedex, France

12 ³Institute of Petroleum Geology and Geophysics, Siberian Branch of Russian Academy of
13 Sciences, Ac. Koptyg av.3, Novosibirsk 90, 630090, Russia

14 ⁴Geological Institute of Russian Academy of Sciences, 7 Pyzhevskii Lane, Moscow, 119017,
15 Russia

16 ⁵UMR 7193 iSTeP UPMC-Univ. Paris 06, CNRS, 4 place Jussieu, F-75252 Paris Cedex 05,
17 France

18 ⁶Institute of Mineralogy and Geochemistry, University of Lausanne, Anthropôle, CH-1015
19 Lausanne, Switzerland

20 ⁷The Institute of Diamond and Precious Metal Geology, Siberian Branch of Russian Academy
21 of Sciences, Lenina av.39, Yakutsk, 677891, Russia

22 ⁸British Geological Survey, Kingsley Dunham Centre, Keyworth, Nottingham NG12 5GG,
23 United Kingdom

24 ⁹Also at Institut Universitaire de France, Paris, France

25

26 † Corresponding author. E-mail: suan@em.uni-frankfurt.de. Present address: Institute of
27 Geosciences, Goethe University Frankfurt, Altenhöferallee 1, D-60438, Frankfurt am Main,
28 Germany

29

30 **Keywords:** Oceanic Anoxic Event, Pliensbachian-Toarcian, carbon isotope excursion, Arctic
31 climate, sea level changes

32 The Toarcian Oceanic Anoxic Event (T-OAE) (ca. 182 mya, Early Jurassic) represents one of
33 the best-recognized examples of greenhouse warming, decreased seawater oxygenation and
34 mass extinction. The leading hypothesis to explain these changes is the massive injection of
35 thermogenic or gas hydrate-derived ^{13}C -depleted carbon into the atmosphere, resulting in a >3
36 per mil negative carbon isotope excursion (CIE), accelerated nutrient input and dissolved
37 oxygen consumption in the oceans. Nevertheless, the lack of a precisely dated record of the T-
38 OAE outside low latitudes has led to considerable debate about both its temporal and spatial
39 extent and hence concerning its underlying causes. Here we present new isotopic and
40 lithological data from three precisely dated N Siberian sections, which demonstrate that mass
41 extinction and onset of strong oxygen-deficiency occurred near synchronously in polar and
42 most tropical sites and were intimately linked to the onset of a marked 6‰ negative CIE
43 recorded by bulk organic carbon. Rock Eval pyrolysis data from Siberia and comparisons
44 with low latitudes show that the CIE cannot be explained by the extent of stratification of the
45 studied basins or changes in organic matter sourcing and suggest that the negative CIE
46 reflects rapid ^{13}C -depleted carbon injection to all exchangeable reservoirs. Sedimentological
47 and palynological indicators show that the injection coincided with a change from cold
48 (abundant glendonites and exotic boulder-sized clasts) to exceptionally warm conditions
49 (dominance of the thermophyllic pollen genus *Classopollis*) in the Arctic, which likely
50 triggered a rapid, possibly partly glacioeustatic sea-level rise. Comparisons with low latitude
51 records reveal that warm climate conditions and poor marine oxygenation persisted in
52 continental margins at least 600 ky after the CIE, features that can be attributed to protracted
53 and massive volcanic carbon dioxide degassing. Our data reveal that the T-OAE profoundly
54 affected Arctic climate and oceanography and suggest that the CIE was a consequence of
55 global and massive ^{13}C -depleted carbon injection.

56
57

58 **1. Introduction**

59

60 Stable carbon isotope ($\delta^{13}\text{C}$) records of carbonate, marine and terrestrial organic carbon
61 show a prominent >3‰ negative carbon isotope excursion (CIE) across an episode of
62 enhanced marine organic carbon deposition termed the Toarcian Oceanic Anoxic Event (T-
63 OAE) (Jenkyns, 1988; Hesselbo et al., 2000, 2007; Kemp et al., 2005; Cohen et al., 2007;
64 Hesselbo and Pieńkowski, 2011). The CIE has been interpreted as reflecting a massive
65 injection of ^{13}C -depleted carbon, either derived from gas hydrates (Hesselbo et al., 2000;

66 Kemp et al., 2005; Cohen et al., 2004, 2007; Hesselbo et al., 2007; Hesselbo and Pieńkowski,
67 2011) or thermogenic methane (Svenson et al., 2007; Mazzini et al., 2010; but see also
68 Gröcke et al., 2009), to the ocean-atmosphere reservoirs. This injection is thought to have
69 promoted, through enhanced greenhouse conditions, a rise in seawater temperatures larger
70 than 6°C, widespread oxygen depletion and severe biotic extinctions among marine
71 invertebrates (Wignall et al., 2005; Kemp et al., 2005; Cohen et al., 2007; Gómez et al., 2008;
72 Caswell et al., 2009; Suan et al., 2010; Jenkyns, 2010; Hesselbo and Pieńkowski, 2011; Dera
73 et al., 2011).

74 Even though the main aspects of the T-OAE are well documented at low latitudes
75 (20–35°N), very few data are available outside the western margin of the Tethyan Ocean,
76 resulting in large uncertainties concerning the cause of the inferred perturbations (Wignall et
77 al., 2005; van de Schootbrugge et al., 2005; Gómez et al., 2008; McArthur et al., 2008). For
78 instance, several authors have argued that anoxic conditions developed only locally and
79 mostly diachronously across European shelves (e.g., van de Schootbrugge et al., 2005;
80 Wignall et al., 2005) and thus were not intimately implicated in the mass extinction (Gómez
81 et al., 2008; Gómez and Goy, 2011). Similarly, the negative CIE has only been observed in a
82 few well dated and continuous sections outside Europe (Bodin et al., 2010; Caruthers et al.,
83 2011) and is absent in belemnite $\delta^{13}\text{C}$ records of the T-OAE, thereby casting doubt on the
84 global expression of the isotopic perturbations (Wignall et al., 2005; van de Schootbrugge et
85 al., 2005). On the other hand, belemnites are extremely scarce during the crucial interval (van
86 de Schootbrugge et al., 2005; Hesselbo et al., 2007; Gómez et al., 2008) and hence may not
87 fully record the details of seawater carbon isotope fluctuations across the T-OAE (Hesselbo et
88 al., 2007).

89 A negative CIE has been recently reported in two different marine Toarcian successions
90 from Argentina (Al-Suwaidi et al., 2010; Mazzini et al., 2010), providing the first southern
91 hemisphere records of the event and substantiating the global significance of the carbon cycle
92 perturbation. Nevertheless, a comprehensive appraisal of the expression of the T-OAE in
93 Argentina is precluded by a major hiatus in the section studied by Al-Suwaidi et al. (2010)
94 and the lack of zonal level ammonite biostratigraphical control in that of Mazzini et al.
95 (2010). Moreover, the relationships between the CIE, the onset of black shale deposition and
96 the extinction event have only been documented in low latitude NW European sections (e.g.,
97 Wignall et al., 2005; Caswell et al., 2009), resulting in large uncertainties concerning the
98 timing between biotic loss, decreased seawater oxygenation and changes in carbon cycling at
99 a global scale.

100 We present new lithological and geochemical data generated from three high latitude
101 marginal marine sections exposed in N Siberia to reconstruct the sea level, carbon cycling and
102 redox history from the Late Pliensbachian to the Late Toarcian in Arctic basins. The ages of
103 the sections are well-constrained based on ammonite, bivalve, dinoflagellate cyst and
104 foraminiferal species that are well correlated to the standard European ammonite zones (Figs.
105 1, 2A). The new data allow the deciphering of regional and global aspects of environmental
106 changes associated with the T-OAE as well as addressing important questions about climate
107 and biotic changes in the Arctic regions throughout this key interval.

108
109

110 **2. Depositional setting and biostratigraphy**

111

112 *2.1. Lithostratigraphy*

113

114 The Anabar Bay, Kelimyar River and Polovinnaya River localities expose Pliensbachian-
115 Toarcian marine successions of sandstone, siltstone and mudstone that were deposited near
116 the Early Jurassic North Pole (Fig. 1). The successions studied at **Anabar Bay** and **Kelimyar**
117 **River** correspond, respectively, to sections 11-12 and 16 of Knyazev et al. (2003). The lower
118 parts of the measured sections at **Anabar Bay** and **Polovinnaya River** (Airkat Formation; Fig.
119 1C) consist of interbedded sandstone, siltstone and silty clay of latest Pliensbachian age,
120 locally rich in large glendonites ($\varnothing > 5$ cm) at **Anabar Bay** (Figs. 1, 2B). Equivalent levels at
121 **Kelimyar River** (Kyra Formation; Fig. 2B) are represented by a succession of siltstone and
122 sandy siltstone with occasional, exotic boulder-sized clasts (composed of limestone, marly
123 limestone and basalts) that are frequently encrusted by bivalves (Figs. 2B, 3). Similar, pebble
124 to boulder-sized exotic clasts were commonly observed throughout the upper 25 m of the
125 Kyra Formation in all nearby successions of the Olenek-Kelimyar Rivers (Devyatov et al.,
126 2010). At **Polovinnaya River**, the presence of abundant macroscopic wood pieces and 2–3 cm
127 pebbles above the wavy and oxidized unconformity between the sandstone beds of Beds 1 and
128 2 indicate that emersion and subaerial erosion were likely to have occurred at this level (Fig.
129 2B). This, together with the overall coarser nature of the exposed sediments compared to
130 **Anabar Bay** and **Kelimyar River**, point to shallowest depositional conditions at **Polovinnaya**
131 **River**. By contrast, the overall finer nature of the sediments at **Kelimyar River** as compared to
132 the two other sections suggests deposition under substantially deeper conditions or at greater
133 distance from major sediment source areas (Fig. 2B). However, a major hiatus is recorded at

134 the Pliensbachian-Toarcian transition in coeval sections near the **Kelimyar River** section
135 (Olenek-Kelimyar Rivers), implying that the depositional depth in the area was sufficiently
136 low to enable subaerial erosion/non deposition during the sea-level fall (Fig. 2B). These
137 lithological trends indicate that the **Polovinnaya River, Anabar Bay** and **Kelimyar River**
138 successions were deposited in shallow, intermediate and deep continental shelf environments
139 respectively.

140 The overlying Kiterbyut Formation at **Polovinnaya River** and **Anabar Bay** comprises dark
141 grey mudstone likely deposited at much greater depths than the underlying sandstone and
142 siltstone, thus signifying substantial sea-level rise. Sediment starvation and accelerated rates
143 of sea-level rise are indicated by high concentrations of belemnite rostra at \sim -0.20 m and \sim 9
144 m at **Polovinnaya River** and 2.5 m at **Anabar Bay** (Fig. 2B). Coeval beds of the Kurung
145 Member at **Kelimyar River** comprise finely laminated, black to brownish shale with large
146 calcareous concretions in the lowermost part of the section. The upper parts of the **Anabar**
147 **Bay** (Eren Formation) and **Kelimyar River** (Kelimyar Formation) sections comprise a
148 succession of siltstone and sandstone that indicate a return to shallower conditions. The
149 macrofauna at **Polovinnaya River** and **Anabar Bay** is represented by abundant thin-shelled
150 bivalves, fish debris, corroded and partly silicified belemnite rostra and poorly preserved
151 ammonites. The **Kelimyar River** section yielded several well-preserved, identifiable
152 ammonites, brachiopods, bivalves and abundant belemnite rostra.

153

154 2.2. Biostratigraphy

155

156 The biostratigraphical framework of the sections investigated is based on ammonites,
157 dinoflagellate cysts, benthic foraminifera and bivalves. **Polovinnaya River** samples were also
158 investigated for calcareous nannofossils but no identifiable specimens were recovered. The
159 ammonite biostratigraphy of the **Kelimyar River** section is relatively well constrained due to
160 the occurrence of a number of key diagnostic species at several horizons (Fig. 2A, B).

161 Additional biostratigraphical resolution was obtained from recent investigations of
162 foraminifera and dinoflagellate cysts developed for the Pliensbachian-Toarcian sections near
163 the Kelimyar and Olenek Rivers and from coeval ammonite-rich sections (Knyazev et al.,
164 2003; Nikitenko, 2008, 2009) of northeast Russia (Astronomicheskaya and Saturn Rivers)
165 (Fig. 1B). According to biostratigraphical schemes developed for NE Russia (Nikitenko,
166 2009), the JF9a-JF9b foraminifera zone boundary identified at 0 m corresponds to the
167 Pliensbachian-Toarcian boundary (*viligaensis-antiquum* ammonite zones) while the JF9a-

168 JF11 boundary identified at 0.12 m corresponds to the *antiquum-falciferum* boundary. Recent
169 collecting in nearby coeval successions (Fig. 2A) indicates that the first occurrence (FO) of
170 the ammonite *Dactylioceras commune* approximates to that of the dinoflagellate cyst
171 *Nannoceratopsis gracilis* (NSJ2), while the FO of the ammonite *Pseudolioceras compactile*
172 (Late Toarcian) coincides with that of the dinoflagellate cysts *Valvaedinium aquilonium* and
173 *Nannoceratopsis triangulata* (NSJ3b). Accordingly, the respective bases of the *commune* and
174 *compactile* zones at **Kelimyar River** can be confidently placed at 3.9 m and 11.8 m (Fig. 2B).

175 Due to the absence of identifiable ammonites in the interval studied at **Anabar Bay** and
176 **Polovinnaya River**, the biostratigraphy of these sections is based on dinoflagellate cysts,
177 benthic foraminifera and bivalves (Fig. 2A) (Zakharov et al., 1997; Riding et al., 1999;
178 Nikitenko and Mickey, 2004; Nikitenko, 2008, 2009). The presence of foraminifera
179 diagnostic of the JF8 and JF9a zones (Nikitenko, 2009) in the sandstone and siltstones of the
180 Airkat Formation at **Anabar Bay** indicates that the measured interval of the Airkat Formation
181 is of Late Pliensbachian age (*margaritatus-viligaensis* zones). Occurrences of the bivalves of
182 the *Tancredia kuznetsovi* bivalve subzone further suggest that this interval is the time
183 equivalent of the *viligaensis* zone (Shurygin, 2005). The absence of diagnostic foraminifera of
184 the JF9b zone indicates that the interval corresponding to the *antiquum* ammonite zone is
185 probably entirely missing in both sections. The placement of the base of the Lower Toarcian
186 in both sections relies on the occurrences of foraminifera diagnostic of the JF11 zone and the
187 bivalve *Dacryomya inflata* (Knyazev et al., 2003; Nikitenko and Mickey, 2004). At
188 **Polovinnaya River**, the interval above ~9 m yielded only non-diagnostic foraminifera. The
189 dinoflagellate cyst *Nannoceratopsis gracilis* was not observed in the entire section, however
190 questionable specimens of *Valvaedinium aquilonium* occur at 13.5 m, suggesting that the
191 upper part of the **Polovinnaya River** section could be of latest Early Toarcian-Late Toarcian
192 age (Fig. 2A, B). Hence, the NSJ2 zone may be entirely missing at **Polovinnaya River**,
193 implying the presence of a major hiatus above 9 m (Fig. 2B).

194

195 **3. Material and methods**

196

197 *3.1. Organic geochemistry*

198

199 Decarbonated and oven-dried sediment samples were analyzed for Total Organic Carbon
200 content (TOC in wt.%) and their stable carbon isotope composition ($\delta^{13}\text{C}_{\text{TOC}}$) with an
201 Eurovector Elemental Analyzer (EuroEA3028-HT) connected to a GV instrument Isoprime

202 isotope ratio mass spectrometer at the University of Lyon 1 (**Polovinnaya River** samples) and
203 with a Carlo Erba 1108 elemental analyzer connected to a Finnigan Delta V isotope ratio
204 mass spectrometer at the University of Lausanne (**Anabar Bay** and **Kelimyar River** samples).
205 The stable carbon isotope ratios are reported in the delta notation as the per mil (‰) deviation
206 relative to the Vienna Pee Dee belemnite (VPDB) standard: $\delta = (R_{\text{sample}} - R_{\text{standard}})/R_{\text{standard}} \times$
207 1000 with $R = {}^{13}\text{C}/{}^{12}\text{C}$. Analytical precision and accuracy were determined by replicate
208 analyses and by comparison with international and in-house standards (IAEA CH7 and
209 tyrosine at the University of Lyon 1; USGS 24, UREA, glycine and pyridine at the University
210 of Lausanne), and were better than 0.1 wt.% (1σ) and 0.1‰ (1σ) for TOC and $\delta^{13}\text{C}_{\text{TOC}}$,
211 respectively.

212

213 *3.2. Rock-Eval pyrolysis*

214

215 Information on the type and thermal maturity of the bulk organic matter was obtained by
216 Rock-Eval pyrolysis using a RE 6 Turbo device at the University Paris 6 (**Polovinnaya River**
217 samples) and RE 6 device at the University of Lausanne (**Kelimyar River** samples) under
218 standard conditions (Béhar et al., 2001). The Hydrogen Index (HI, mg HC/g TOC), Oxygen
219 Index (OI, mg CO₂/g TOC), Tmax (°C) and TOC (wt.%) were determined. Analytical
220 precision was better than 0.05 wt.% (1σ) for TOC, 1.5°C (1σ) for Tmax, 10 mg HC/g TOC
221 (1σ) for HI and 10 mg CO₂/g TOC (1σ) for OI. The TOC contents measured by Rock-Eval
222 pyrolysis were in excellent agreement with those measured during the $\delta^{13}\text{C}_{\text{TOC}}$ acquisition,
223 with correlation coefficients (R^2) of 0.8 for **Polovinnaya River** samples and 0.97 for **Kelimyar**
224 **River** samples.

225

226 *3.3. Pyrite framboid measurements*

227

228 Smear slides for pyrite framboid measurements were prepared by gentle mechanical
229 breakage of a small amount of rock, dilution with water, spreading onto a coverslip and
230 drying in a stove. The maximum diameter of pyrite framboids from **Polovinnaya River** was
231 measured on images acquired by light microscopy with a CCD camera (Sony XC-77CE
232 mounted on a polarizing microscope ZEISS Axioscope 40). For each horizon, 30 framboids
233 were measured by means of the software Scion Image (beta version 402) with an estimated
234 error of $\pm 0.17 \mu\text{m}$. Fragmented pyrite framboids were not observed while non-framboidal

235 particles exceeding 50 μm were commonly observed during the measurements, indicating that
236 the mechanical breakage did not affect the size distribution of the measured framboids.

237

238

239 4. Results

240

241 4.1. Organic stable carbon isotope and total organic carbon data

242

243 The $\delta^{13}\text{C}_{\text{TOC}}$ and TOC data from the three sections investigated reveal comparable trends
244 (Fig. 4). The deeper and more complete **Kelimyar River** section exhibits a pronounced 6‰
245 negative CIE starting at the boundary of the *antiquum-falciferum* ammonite zones above a
246 major flooding surface and reaching minimum values (-32‰) in the lowermost part of the
247 *falciferum* zone (Fig. 4). Similar trends occur at **Anabar Bay** and **Polovinnaya River**, although
248 the CIE is proportionally reduced and profoundly negative $\delta^{13}\text{C}_{\text{TOC}}$ values ($<-30\text{‰}$) are
249 absent (Fig. 4). In all three sections, the decrease in $\delta^{13}\text{C}_{\text{TOC}}$ at the base of the *falciferum* zone
250 is accompanied by a marked rise in TOC contents. The succeeding interval (*falciferum-*
251 *commune* zones) at **Anabar Bay** and **Kelimyar River** records high TOC, and a corresponding
252 plateau of relatively negative $\delta^{13}\text{C}_{\text{TOC}}$ values. The record at **Kelimyar River** indicates that the
253 end of black shale deposition, and a return to almost pre-excursion values, occurred in the
254 middle of the *commune* zone (Fig. 4). The abrupt $\sim 2\text{‰}$ shift to lighter values recorded at ~ 9 m
255 at **Polovinnaya River** is accompanied by elevated belemnite concentrations (Figs. 2, 4) and
256 most likely reflect a major break in sedimentation. Biostratigraphical data (see part 2.2.)
257 indicate that this shift and the following interval of rather low $\delta^{13}\text{C}_{\text{TOC}}$ values most likely
258 correlate with the $\sim 2\text{‰}$ negative CIE recorded across the Lower-Upper Toarcian transition at
259 **Kelimyar River** (from ~ 8 to ~ 15 m; Fig. 4).

260

261 4.2. Organic matter sourcing

262

263 The crossplots of HI/OI values indicate that the organic matter (OM) mainly consists of
264 hydrogen-poor terrestrial material and altered organic matter (Type III/IV kerogen) in the
265 **Polovinnaya River** section and of a mixture of terrestrial and marine material (Type II/III
266 kerogen) in the **Kelimyar River** section (Fig. 5). This observation is consistent with the more
267 proximal depositional setting inferred for the **Polovinnaya River** site. At both sites, HI values
268 increase across the Pliensbachian-Toarcian boundary, indicating increased contribution of

269 marine material during transgression (Fig. 4). At **Kelimyar River**, lowest $\delta^{13}\text{C}_{\text{TOC}}$ values
270 recorded across the *antiquum-falciferum* boundary correspond to low HI values (30-100 mg
271 HC/gTOC). Importantly, the most ^{13}C -depleted sample ($\delta^{13}\text{C}_{\text{TOC}} = -32\text{‰}$) has a TOC of 3.5
272 wt.%, indicating that its low HI value is unlikely to be the result of intense OM oxidation but
273 most probably reflects a terrestrial-derived OM source (Fig. 4). Highest HI values occur at ~5
274 m and decrease significantly in the upper part of the black shale interval and overlying silty
275 beds (*commune* zone), indicating decreased marine OM sourcing (Fig. 4).

276

277 4.3. Oxygenation

278

279 At all sites, strong oxygen-depletion throughout the interval of high TOC values
280 (*falciferum*-basal *commune* zones; Figs. 2, 4) is indicated by distinct lamination, the sporadic
281 occurrence of monospecific associations of thin-shelled bivalves and thin-valved ostracodes
282 typical of oxygen-poor environments (Nikitenko and Mickey, 2004; Zakharov et al., 2006)
283 and the absence of both endobenthic fauna and bioturbation. The mean size of the pyrite
284 framboids recorded through the *falciferum* and *commune* zones at **Polovinnaya River** (Fig. 4)
285 are lower than 7 μm , consistent with nucleation and growth within a strongly dysaerobic to
286 possibly euxinic environment (Wilkin et al., 1996; Wignall and Newton, 1998). The framboid
287 size distribution indicates that even shallow marine areas became strongly oxygen-depleted at
288 this time. However, lower TOC contents and higher abundance of monospecific thin-shelled
289 bivalves at **Polovinnaya River** indicate longer or more frequent oxygenation events at
290 shallower sites.

291

292

293 5. Discussion

294

295 5.1. Origin of the negative carbon isotope excursion

296

297 The high-resolution biostratigraphical control of our new geochemical data from N Siberia
298 allows a direct comparison with previous records for the T-OAE in order to decipher the
299 global and regional aspects of the event. A marked increase of HI values, likely reflecting
300 increased marine OM preservation or input, has been documented across the onset of the CIE
301 in most records from Europe (e.g., Baudin et al., 1990; Prauss et al., 1991; Röhl et al., 2001;
302 Sabatino et al., 2009). The **Kelimyar River** record, corresponding to the most complete of the

303 three investigated N Siberian sections, indeed reveals an overall increase of HI values across
304 the CIE and thus indicates increased marine OM input during the accompanying transgression
305 (Fig. 4). Because Toarcian marine OM appears to have been more ^{13}C -depleted than terrestrial
306 OM (Hesselbo et al., 2000), the CIE recorded by bulk OM in N Siberia could conceivably
307 reflect changes in the OM sourcing. However, lowest $\delta^{13}\text{C}_{\text{TOC}}$ values ($<-29\%$) recorded
308 across the *antiquum-falciferum* zone transition correspond to low HI values characteristic of
309 terrestrial OM (32 to 100 mgHC/gTOC; Fig. 4), thus ruling out increased marine OM
310 contribution as the main cause of the marked $\delta^{13}\text{C}_{\text{TOC}}$ shift towards lower values at this site.
311 Similarly, the relatively low HI (3 to 91 mgHC/gTOC) values from **Polovinnaya River**
312 correlate poorly with $\delta^{13}\text{C}_{\text{TOC}}$ (Fig. 4), indicating little influence of the type of preserved OM
313 on the recorded isotopic fluctuations. In this regard, the absence of very negative $\delta^{13}\text{C}_{\text{TOC}}$
314 values ($<-30\%$) at the base of the *falciferum* zone at **Polovinnaya River** and **Anabar Bay**
315 might point to a substantial lateral variability of the $\delta^{13}\text{C}_{\text{TOC}}$ signal (Fig. 4). In both sections,
316 however, the marked $\delta^{13}\text{C}_{\text{TOC}}$ shift towards lower values occurs in an interval characterized by
317 elevated belemnite concentrations above a major flooding surface; given the relatively coarse
318 resolution of our sampling (every 0.25 m at **Polovinnaya River** and 0.5 m at **Anabar Bay**), the
319 absence of very negative $\delta^{13}\text{C}_{\text{TOC}}$ values at both sites can more likely be attributed to
320 extremely reduced sedimentation rates or even to non-deposition due to transgression-induced
321 sediment starvation. Importantly, comparison of the biostratigraphically well-constrained
322 succession of **Kelimyar River** with that of SW Germany (where coeval TOC, HI and $\delta^{13}\text{C}_{\text{TOC}}$
323 records are available at sufficiently high resolution) reveals almost identical temporal $\delta^{13}\text{C}_{\text{TOC}}$
324 trends while their HI profiles differ **considerably** (Fig. 6). These observations show that the
325 type of preserved OM has little influence on the recorded isotopic profiles and support the
326 inference that the CIE is not compositionally controlled, as suggested independently by
327 compound-specific $\delta^{13}\text{C}$ data from SW Germany (Schouten et al., 2000).

328 It has been repeatedly proposed that the CIE reflects regional upwelling of mineralized
329 ^{13}C -depleted carbon in salinity-stratified restricted basins (Küspert, 1982; Schouten et al.,
330 2000; van de Schootbrugge et al., 2005; McArthur et al., 2008). In this case, the amount of
331 ^{13}C -depleted carbon recycling would logically have been a function of the extent of
332 stratification and associated amount of available degradable OM and a systematic relationship
333 between the amount of TOC and the magnitude of the CIE should be expected. **The TOC and**
334 **$\delta^{13}\text{C}_{\text{TOC}}$ records from Anabar Bay indeed show a good correlation (Fig. 5), pointing to a**
335 **possible link between the recycling of ^{13}C -depleted carbon and general $\delta^{13}\text{C}_{\text{TOC}}$ trends. The**
336 **correlation between TOC and $\delta^{13}\text{C}_{\text{TOC}}$ is however moderate to poor at Polovinnaya River and**

337 **Kelimyar River (Fig. 5), suggesting a less pronounced overprinting of the $\delta^{13}\text{C}_{\text{TOC}}$ values by**
338 **local ^{13}C -depleted carbon recycling at these localities. In this regard, it is noteworthy that the**
339 TOC-rich interval is about half as thick and the TOC contents approximately half lower in the
340 most complete **Kelimyar River** section than in SW Germany (Fig. 6), implying that the
341 amount of carbon buried per unit of time was at least four times lower in N Siberia than in
342 SW Germany (Fig. 6). Notwithstanding these substantially different rates of carbon burial,
343 both successions record almost identical $\delta^{13}\text{C}_{\text{TOC}}$ values and trends (Fig. 6). Consistent with
344 previous compound-specific and biomarker data from France (van Breugel et al., 2006), this
345 comparison suggests that the magnitude and shape of the CIE **cannot be entirely explained by**
346 the degree of stratification of these basins. Our new N Siberian data indicate that the
347 upwelling of the mineralized ^{13}C -depleted carbon and changes in OM sourcing, **although**
348 **possibly exerting an influence on general $\delta^{13}\text{C}_{\text{TOC}}$ records,** were unlikely to be the main
349 causes of the CIE, and thus support the idea that the CIE reflects a rapid and synchronous
350 injection of ^{13}C -depleted carbon to all exchangeable reservoirs (e.g., Hesselbo et al., 2000,
351 2007; Kemp et al., 2005; Cohen et al., 2007; Hesselbo and Pieńkowski, 2011; **Caruthers et al.,**
352 **2011).** Accordingly and provided that the source of the analyzed carbon and the
353 biostratigraphy are sufficiently well constrained, the CIE might constitute a valuable
354 chemostratigraphic marker between distant sites, with a resolution potentially far higher than
355 that available from ammonite or nannofossil biostratigraphy.

356

357 *5.2. Climatic conditions across the T-OAE in the polar regions*

358

359 Different sedimentological indicators point to cold climate conditions in the Arctic prior to
360 the T-OAE negative CIE and accompanying onset of oxygen-depletion. Cold bottom water
361 temperatures during the Late Pliensbachian are indicated by the occurrence of large ($\varnothing > 5$ cm)
362 glendonites (calcite pseudomorphs after ikaite) in Upper Pliensbachian strata at **Anabar Bay**
363 (Figs. 2, 3) and several other localities in N Siberia (Kaplan, 1978). Indeed, ikaite
364 precipitation in the sediment at the seafloor might be favored by several factors (e.g., high
365 alkalinity, elevated phosphate concentrations), among which temperatures lower than 4°C
366 appear as the most significant, making glendonites robust indicators of cold water conditions
367 (e.g., Bischoff et al., 1993; Selleck et al., 2007). As such, the absence of glendonites in Upper
368 Pliensbachian strata of **Polovinnaya River** and **Kelimyar River** suggests that the conditions
369 favoring ikaite precipitation or its subsequent transformation into pseudomorphic calcite may
370 have only been met in specific areas. The glendonites of **Anabar Bay** occur in sediments

371 deposited at very shallow depths and were thus most likely formed at or above the
372 thermocline, suggesting that sea surface temperatures were at least locally no more than a few
373 degrees higher than the formation temperature of ikaite during this interval. Low sea surface
374 temperatures are consistent with the occurrence of isolated, likely ice-rafted boulders
375 encrusted by *Harpax* bivalves within otherwise homogenous coeval siltstone succession at
376 **Kelimyar River** and in nearby areas (Figs. 2, 3; see also part 2.1.). It has been argued that
377 deposition of similar isolated exotic boulders may have resulted from driftwood rafting and
378 may not necessarily indicate ice transport (Bennett and Doyle, 1996). In this case, boulders
379 transported by driftwood should then also be observed in low latitude epicontinental marine
380 areas surrounded by the large landmasses of the N Tethyan margin, where trees would have
381 been relatively common and the occurrence of driftwood is well documented (e.g., Hesselbo
382 et al., 2007). To our knowledge, however, no such erratic boulders have been reported from
383 contemporaneous European successions, and this despite abundant lithological descriptions of
384 epicontinental Upper Pliensbachian strata (e.g., Howarth, 1985; Hesselbo and Jenkyns, 1995;
385 Suan et al., 2010; van de Schootbrugge et al., 2010). Whilst a driftwood origin cannot be
386 totally excluded, ice transport appears as a more parsimonious explanation given the polar
387 paleolatitude of the sites studied (Fig. 1); the lack of evidence of transport by continental ice
388 such as striation or faceting suggests that these boulders reflect the at least intermittent
389 (possibly seasonal) formation of polar sea ice at this time.

390 Evidence for considerable warming at the *antiquum-falciferum* zone transition is the
391 disappearance of glendonites and exotic boulder-sized clasts and the appearance of low
392 latitude terrestrial plant taxa throughout the Arctic region, including abundant proportions of
393 the thermophyllic (e.g., Traverse, 2007) pollen genus *Classopollis* (Vakhrameev, 1991;
394 Zakharov et al., 2006). Reports of plants of subtropical to tropical affinities (*Ptilophyllum*) in
395 central and NE Siberia additionally suggest an interval of extreme polar to subpolar warmth
396 during the succeeding *falciferum*-early *commune* interval (Vakhrameev, 1991). Indications of
397 unusually warm and humid conditions at slightly lower latitudes also come from reports of
398 weathering crusts of kaolinite and bauxite in Lower Toarcian continental deposits of the W
399 Siberian Basin (Fig. 1; Kontorovich et al., 1997), but these clearly need further documentation
400 and biostratigraphical analyses. The disappearance of abundant *Classopollis* and associated
401 thermophyllic plant elements from the Arctic in the middle part of the *commune* zone
402 (Zakharov et al., 2006) indicates that the termination of black shale deposition probably
403 coincided with a return to substantially cooler conditions (Fig. 6). These sedimentological and
404 palynological data thus point to a dramatic increase of both sea and air temperatures across

405 the T-OAE negative CIE in Arctic areas and indicate that exceptionally warm climate
406 conditions persisted during the following interval of poor marine oxygenation (see part 5.4.).
407

408 5.3. Sea level changes

409

410 The lithological successions of the three sections studied point to significant changes in sea
411 level across the Pliensbachian-Toarcian interval in the Arctic Basin. In all sections, the Upper
412 Pliensbachian is dominated by sandy and silty lithologies suggestive of very shallow
413 depositional conditions, while the Lower Toarcian is dominated by clay lithologies clearly
414 deposited at greater water depths. The major unconformity recorded immediately below the
415 CIE at the Pliensbachian-Toarcian transition in **Anabar Bay** and **Polovinnaya River** sections
416 (Fig. 2) has been documented in the entire Arctic region, and was probably linked to a short-
417 lived episode of subaerial exposure (Nikitenko and Mickey, 2004; Zakharov et al., 2006).
418 Importantly, this unconformity is overlain by fine clay in **Anabar Bay** and **Polovinnaya River**
419 sections, suggesting that the sea level rose markedly and relatively rapidly across the CIE. It
420 should be noted that a similar history of sea-level changes has been inferred from coeval
421 foraminifera and ostracode assemblages from the entire Arctic region (Nikitenko, 2009), thus
422 ruling out changing sediment supply as the main cause of these lithological changes.

423 Significantly, the condensed lowermost part of the CIE in shallow marine sites of N
424 Siberia is strikingly similar to that recorded in tropical shallow marine sites (van Breugel et
425 al., 2006) (Fig. 7). As observed in N Siberia, the earliest Toarcian ammonite zone (the
426 *tenuicostatum* zone) is also frequently reduced or even absent in NW Europe, so that T-OAE
427 organic-rich sediments often unconformably rest on Upper Pliensbachian strata in several
428 sections in England (Wignall, 1991), S France (Guex et al., 2001; Léonide et al., in press) and
429 Germany (Röhl and Schmid-Röhl, 2005). These observations indicate synchronicity of sea
430 level changes in distant (>5,000 km) areas and indicate that the massive ¹³C-depleted carbon
431 injection at the *antiquum-falciferum* zone transition coincided with a dramatic eustatic sea
432 level rise following a major generalized regression. The short duration (80–150 kyr) of the
433 $\delta^{13}\text{C}_{\text{TOC}}$ decrease (Kemp et al., 2005; Cohen et al., 2007; Suan et al., 2008; Sabatino et al.,
434 2009) additionally suggests that the transgression was extremely rapid and hence most likely
435 to have been climate-driven. The study of European sections with slightly different lithologies
436 suggests that sea level rose by about 30-90 m between the deposition of uppermost
437 Pliensbachian shallow-water sediments and that of organic-rich mudstones recording the CIE
438 (Hallam, 1997). The 6–10°C warming recorded across the T-OAE (Bailey et al., 2003;

439 Gómez et al., 2008; Suan et al., 2010), through thermal expansion (Revelle, 1990), may
440 explain a 3–10 m sea-level rise, suggesting that several meters of sea level rise may have been
441 related to the massive melting of continental ice. This latter explanation is compatible with
442 evidence for near-freezing conditions in the pre-CIE interval of the sections studied (see part
443 5.2.; Fig. 4), and rapid cooling and widespread sea level fall during the Late Pliensbachian-
444 earliest Toarcian (Guex et al., 2001; Suan et al., 2010). Additionally, compelling evidence for
445 rapid and large, probably glacially induced sea level fluctuations immediately prior to the T-
446 OAE lies in the identification of a series of incised valleys ranging from 20 to 50 m in depth
447 within Upper Pliensbachian (*margaritatus* and *spinatum* zones) and lowermost Toarcian (intra
448 *tenuicostatum* zone) offshore marine sediments from the North Sea (Marjanac and Steel,
449 1997). In this context, records of abundant and diverse Pliensbachian pollen and spore
450 assemblages, and the lack of coeval voluminous glacial deposits (Zakharov et al., 2006),
451 suggest that continental areas close to the North Pole remained largely ice-free during the
452 entire Pliensbachian-Toarcian interval. Accordingly, any substantially large, pre-T-OAE
453 icecap would most probably have been located in the high-latitude large landmasses of the
454 southern hemisphere.

455

456 5.4. Timing and causes of oxygen depletion during the T-OAE

457

458 The association between the 6‰ negative CIE and the marked TOC rise at the *antiquum-*
459 *falciferum* zone transition recorded in the more complete **Kelimyar River** section coincides
460 precisely with that recorded at the *tenuicostatum-falciferum* zone transition or their
461 equivalents in several low-latitude sites (Küspert, 1982; Hesselbo et al., 2000; Röhl et al.,
462 2001; Prauss et al., 1991; van Breugel et al., 2006) (Figs. 6, 7). A similar succession of
463 environmental change was recently reported in Argentina, although a hiatus prevents
464 appraisal of post-CIE conditions in the section studied (Al-Suwaidi et al., 2010). **In the**
465 **Arctic, the interval recording high TOC values and decreased oxygenation is considerably**
466 **expanded compared to that recording the negative CIE (Figs. 3, 6). A strikingly similar**
467 **pattern is also present in many epicontinental sections from NW Europe (Fig. 7; Küspert,**
468 **1982; Röhl et al., 2001; McArthur et al., 2008; van Breugel et al., 2006), thus signifying**
469 **stressful environmental perturbation for some considerable time after the end of the CIE. In**
470 **more open marine records from S Europe, however, high TOC and evidence for poor**
471 **oxygenation appear to be generally restricted to the CIE (Fig. 7; Parisi et al., 1996; Mattioli et**
472 **al., 2004; Sabatino et al., 2009; Kafousia et al., 2011). Assuming that the CIE represents a**

473 good time marker (Hesselbo et al., 2007; Hesselbo and Pieńkowski, 2011; Caruthers et al.,
474 2011; see part 5.1.), our new records from N Siberia therefore imply that oxygen-depletion
475 developed near synchronously in most considered areas but faded away later in areas close to
476 the large northern emergent landmasses of N Siberia and NW Europe. In addition, we note
477 that some biostratigraphically well-constrained Lower Toarcian sections from southern
478 Europe are essentially devoid of black shales or evidence of strong oxygen-depletion (e.g.,
479 Hesselbo et al., 2007; Gómez and Goy, 2011). These observations, combined to our new
480 Siberian data, therefore imply that strong oxygen-deficiency was a widespread response of
481 epicontinental seas to Toarcian climate changes, but suggests that both its timing and
482 intensity, as suggested for most other OAEs (e.g., Jenkyns, 2010), may have been locally
483 strongly modulated by regional factors.

484 Interestingly, clay mineral assemblages and oxygen isotope compositions of different
485 biogenic material (carbonate of belemnites and brachiopods, phosphate of fish apatite), along
486 with Mg/Ca ratios of belemnites, indicate that the maximum development of oxygen-
487 depletion during the early *falciferum* zone occurred at times of exceptionally warm and humid
488 conditions (Fig. 5; Rosales et al., 2006; Dera et al., 2009; Suan et al., 2010; Dera et al., 2011).
489 Accordingly, widespread development of seawater oxygen-depletion in both polar and
490 subtropical marginal shelves during the early *falciferum* zone interval likely resulted from
491 density stratification and increased productivity due to an accelerated hydrological cycle
492 under warm climate and elevated CO₂ concentrations (e.g., Cohen et al., 2007; Dera et al.,
493 2009; Jenkyns, 2010). In this regard, evidence for cold, possibly near-freezing conditions
494 before the T-OAE in the Arctic is equally very significant because it supports the view that
495 Arctic shelves were major sites of oxygen-rich, cold and deep water formation during at least
496 parts of the Early Jurassic (Wignall et al., 2010). If correct, reduced pole-to-equator thermal
497 gradients and increased freshwater runoff in Arctic regions during the early *falciferum* zone
498 were likely to have decreased or shut down this formation of oxygen-rich deep waters, and
499 could then have further contributed to oxygen-depletion in more open-ocean settings during
500 peak warmth. Because seawater anoxia in open ocean settings may also result from elevated
501 nutrient loads (Meyer and Kump, 2008), further modeling is required to constrain the
502 respective role of changes in nutrient inputs, high-latitude oxygen solubility and polar deep
503 water formation on global oceanic oxygenation during the T-OAE.

504 Clay mineral assemblages, oxygen isotope and Mg/Ca ratios show that humidity and
505 seawater temperatures decreased substantially during the following *falciferum-bifrons* zones,
506 though not returning to pre-CIE conditions (Fig. 6; see Dera et al., 2009 and references

507 therein). As global temperatures and weathering rates decreased during the *falciferum* zone
508 (Fig. 6), seawater oxygen-depletion probably gradually decreased in areal extent and became
509 restricted to more sensitive areas close to large landmasses (i.e., the Arctic and the N Tethyan
510 margin). At both polar and subtropical latitudes, the thickness of the interval showing
511 evidence of poor oxygenation and high TOC is approximately twice that of the negative CIE
512 (Fig. 5). The duration of the CIE has been estimated at between ~300 and ~900 ky (Kemp et
513 al., 2005; Cohen et al., 2007; Suan et al., 2008). Assuming constant sedimentation rates for
514 the black shale intervals at **Kelimyar River** and in southwest Germany (Fig. 6), elevated
515 carbon burial and high temperatures thus persisted between 600 and 1,800 ky after the end of
516 the CIE. If temperatures were CO₂-forced during this interval (Fig. 6), this implies that
517 widespread elevated carbon burial in marine realms was largely overcompensated by
518 additional CO₂ input. Such massive and long-lived carbon injection appears unlikely to have
519 been caused solely by gas hydrate dissociation, but is instead compatible with the known
520 protracted (>3 My) range of activity of the Karoo-Ferrar large igneous province (e.g., Jourdan
521 et al., 2008).

522

523 5.5. Timing and causes of biotic turnover

524

525 Previous studies of fossil range data from the Arctic documented two main extinction
526 horizons of different magnitude across the Pliensbachian-Toarcian interval (Nikitenko and
527 Mickey, 2004; Zakharov et al., 2006; Nikitenko, 2008). A first extinction horizon was
528 documented among several marine groups across the *viligaensis-antiquum* zone transition of
529 NE Russia (Zakharov et al., 2006), which might correlate with that recorded at the
530 Pliensbachian-Toarcian transition in Europe (Wignall et al., 2005; Caswell et al., 2009).
531 However, the reduced thickness or absence of this interval in the sites studied herein hampers
532 appraisal of the accompanying environmental changes in the Arctic. A second extinction
533 horizon of higher magnitude, involving a complete reorganization of bivalve, ostracode,
534 benthic foraminifera, pollen and spore assemblages has been previously identified over the
535 entire Arctic basin at the *antiquum-falciferum* zone transition (Nikitenko and Mickey, 2004;
536 Zakharov et al., 2006; Nikitenko, 2008), and hence correlates with the prominent $\delta^{13}\text{C}_{\text{TOC}}$ fall
537 the base of the CIE in our more complete **Kelimyar River** record (Fig. 6). In low latitude sites,
538 macrofossil and microfossil data place the main marine extinction horizon slightly below or
539 within the $\delta^{13}\text{C}_{\text{TOC}}$ fall (Wignall et al., 2005; Boomer et al., 2008; Caswell et al., 2009;
540 Gómez and Goy, 2011).

541 Assuming that the CIE does reflect a synchronous and global event (see part 5.1.), the main
542 extinction episode thus appears to have been broadly synchronous between Arctic and low
543 latitude sites (Fig. 6). The close association between the extinctions and the $\delta^{13}\text{C}_{\text{TOC}}$ fall in
544 both regions suggests that biotic losses **may have been caused by environmental changes**
545 **directly ensuing from massive ^{13}C -depleted carbon injection**. Nevertheless, macrofossil range
546 data from the well-studied sections of the Yorkshire coast place the extinction horizon of
547 many invertebrates slightly below the $\delta^{13}\text{C}_{\text{TOC}}$ fall in the upper *tenuicostatum* zone,
548 suggesting that some biotic losses predated the CIE and were thus unrelated to the ^{13}C -
549 depleted carbon injection (Wignall et al., 2005; Caswell et al., 2009). Unfortunately, the
550 resolution of our sampling of the stratigraphically very reduced *antiquum* zone in **Kelimyar**
551 **River** is too coarse **to investigate the detailed stratigraphic relationships between the CIE and**
552 **extinctions**, while the Arctic sections from NE Russia characterized by an expanded
553 *antiquum-falciferum* zone transition (where the details of the extinctions could be potentially
554 best seen) currently lack $\delta^{13}\text{C}$ records and have relatively low resolution biotic records (e.g.,
555 Knyazev et al., 2003; Nikitenko and Mickey, 2004). Further detailed geochemical and
556 paleontological investigations are thus needed to better constrain the precise timing, and
557 hence cause-and-effects relationships, between carbon injection and biotic turnover in both
558 high- and low-latitude areas during this crucial interval.

559

560

561 **6. Conclusions**

562

563 An abrupt 6‰ negative CIE is revealed in bulk organic carbon during the onset of the T-
564 OAE from biostratigraphically well constrained marine sections deposited at polar
565 paleolatitudes. Rock Eval pyrolysis and comparisons with tropical paleolatitudes indicate that
566 changing OM sources and basin restriction were very unlikely to be the main causes of the T-
567 OAE negative CIE and support the hypothesis that the isotopic anomaly reflects a massive
568 and rapid injection of ^{13}C -depleted carbon into ocean-atmosphere system. Lithological and
569 paleontological data from the Arctic indicate that this injection coincided with changes from
570 cold to exceptionally warm climate and the onset of marine oxygen deficiency. Evidence for
571 near-freezing climate conditions in the Arctic before the T-OAE (i.e., exotic boulder-sized
572 clasts and large glendonites) suggests that the rapid sea level rise recorded in both domain
573 during the carbon injection was caused by a combination of thermal expansion of seawater
574 and massive and rapid melting of continental ice. The persistence of warm climate and poorly

575 oxygenated conditions more than 600 ky after the CIE at both polar and tropical sites
576 indicates prolonged carbon injection despite concomitant elevated redox-driven carbon burial,
577 consistent with a massive and protracted input of volcanogenic carbon. The main phase of
578 marine biota extinction appears to have been closely related with the onset of massive ¹³C-
579 depleted carbon injection in both Arctic and low latitude sites, but further work is required to
580 constrain cause-and-effects relationships between warming, massive carbon injection and
581 perturbation of both marine and terrestrial ecosystems across the T-OAE.

582

583 **Acknowledgments**

584 We are grateful to F. Fourel and B. Bomou for laboratory assistance and to P. Wignall, B.
585 Gill and anonymous reviewers for their **helpful** comments on earlier versions of this
586 manuscript. This work was supported by RAS projects numbers 17 and 24, the CUS Geonova
587 project and the Regional Geological and Geophysical Studies of the Siberian Arctic
588 Continental Margin Project funded by TGS-NOPEC Geophysical Company. J.B.R. publishes
589 with the approval of the Executive Director, British Geological Survey (NERC).

590

591 **References**

- 592 Al-Suwaidi, A.H., Angelozzi, G.N., Baudin, F., Damborenea, S.E., Hesselbo, S.P., Jenkyns,
593 H.C., Manceñido, M.O., Riccardi, A.C., 2010. First record of the Early Toarcian
594 Oceanic Anoxic Event from the Southern Hemisphere, Neuquén Basin, Argentina. *J.*
595 *Geol. Soc. London* 167, 633–636.
- 596 Baudin F., Herbin, J-P., Vandenbroucke, M. 1990. Mapping and geochemical characterization
597 of Toarcian organic matter in the Mediterranean Tethys. *Organic Geochemistry* 16,
598 677–687.
- 599 Bailey, T.R., Rosenthal, Y., McArthur, J.M., van de Schootbrugge, B., Thirlwall, M.F., 2003.
600 Paleooceanographic changes of the Late Pliensbachian-Early Toarcian interval: a possible
601 link to the genesis of an Oceanic Anoxic Event. *Earth Planet. Sci. Lett.* 212, 307–320.
- 602 Béhar, F, Beaumont, V., De B. Penteadó, H.L., 2001. Rock-Eval 6 Technology: Performances
603 and Developments: Oil & Gas Science and Technology. *Revue de l'IFP* 56, 111–134.
- 604 Bennett, M.R., Doyle, P., 1996. Global cooling inferred from dropstones in the Cretaceous:
605 fact or wishful thinking? *Terra Nova* 8, 182–185.
- 606 Bilotta, M., Venturi, F., Sassaroli, S., 2010. Ammonite faunas, OAE and the Pliensbachian–
607 Toarcian boundary (Early Jurassic) in the Apennines. *Lethaia* 43, 357–380.

- 608 Bischoff, J.L., Fitzpatrick, J.A., Rosenbauer, R.J., 1993. The solubility and stabilization of
609 ikaite (CaCO₃-6H₂O) from 0° to 25°C; environmental and paleoclimatic implications
610 for thynolite tufa. *J. Geol.* 101, 21–33.
- 611 Bodin, S., Mattioli, E., Fröhlich, S., Marshall, J.D., Boutib, L., Lahsini, S., Redfern, J., 2010.
612 Toarcian carbon isotope shifts and nutrient changes from the Northern margin of
613 Gondwana (High Atlas, Morocco, Jurassic): palaeoenvironmental implications.
614 *Palaeogeogr. Palaeoclimatol. Palaeoecol.* 297, 377–390.
- 615 Caruthers, A.H., Gröcke, D.R., Smith, P.L., 2011. The significance of an Early Jurassic
616 (Toarcian) carbon-isotope excursion in Haida Gwaii (Queen Charlotte Islands), British
617 Columbia, Canada. *Earth Planet. Sci. Lett.* 307, 19–26
- 618 Caswell, B.A., Coe, A.L., Cohen, A.S., 2009. New range data for marine invertebrate species
619 across the early Toarcian (Early Jurassic) mass extinction. *J. Geol. Soc. London* 166,
620 859–872.
- 621 Cohen, A.S., Coe, A.L., Harding, S.M., Schwark L., 2004, Osmium isotope evidence for the
622 regulation of atmospheric CO₂ by continental weathering. *Geology* 32, 157–160.
- 623 Cohen, A.S., Coe, A.L., Kemp, D.B., 2007. The Late Palaeocene–Early Eocene and Toarcian
624 (Early Jurassic) carbon isotope excursions: a comparison of their time scales, associated
625 environmental changes, causes and consequences. *J. Geol. Soc. London* 164, 1093–
626 1108.
- 627 Dera, G., Pellenard, P., Neige, P., Deconinck, J.-F., Pucéat, E., Dommergues, J.-L., 2009.
628 Distribution of clay minerals in Early Jurassic Peritethyan seas: palaeoclimatic
629 significance inferred from multiproxy comparisons. *Palaeogeogr. Palaeoclimatol.*
630 *Palaeoecol.* 271, 39–51.
- 631 Dera, G., Brigaud, B., Monna, F., Laffont, R., Pucéat, E., Deconinck, J.-F., Pellenard, P.,
632 Joachimski, M.M., Durlet, C., 2011. Climatic ups and downs in disturbed Jurassic
633 world, *Geology* 39, 215–218.
- 634 Devyatov, V.P., Knyazev, V.G., Nikitenko, B.L., Melnik, O.A., Glinskikh, L.A., 2010.
635 Pliensbachian – Toarcian boundary of northeastern Siberia and stratigraphic position of
636 the Kurung Mbr of the Kelimyar Formation (Kelimyar River, Olenek River basin).
637 *Otechestvennaya geologiya* 5, 105–112.
- 638 Gómez, J.J., Goy, A., 2011. Warming-driven mass extinction in the Early Toarcian (Early
639 Jurassic) of northern and central Spain. Correlation with other time-equivalent European
640 sections. *Palaeogeogr. Palaeoclimatol. Palaeoecol.* 306, 176–195

641 Gómez, J.J., Goy, A., Canales, M.L., 2008. Seawater temperature and carbon isotope
642 variations in belemnites linked to mass extinction during the Toarcian (Early Jurassic)
643 in Central and Northern Spain. Comparison with other European sections. *Palaeogeogr.*
644 *Palaeoclimatol. Palaeoecol.* 258, 28–58.

645 Gröcke, D.R., Rimmer, S.M., Yoksoulia, L.E., Cairncross, B., Tsikos, H., van Hunen, J.,
646 2009. No evidence for thermogenic methane release in coal from the Karoo-Ferrar large
647 igneous province. *Earth Planet. Sci. Lett.* 277, 204–212.

648 Guex, J., Morard, A., Bartolini, A., Morettini, E., 2001. Découverte d’une importante lacune
649 stratigraphique à la limite Domérien-Toarcien: implications paléo-océanographiques.
650 *Bulletin de la Société Vaudoise des Sciences Naturelles* 345, 277–284.

651 Hallam, A., 1997. Estimates of the amount and rate of sea-level change across the Rhaetian–
652 Hettangian and Pliensbachian–Toarcian boundaries (latest Triassic to early Jurassic). *J*
653 *Geol. Soc. London* 154, 773–779.

654 Hesselbo, S.P., Jenkyns, H.C., 1995. A comparison of the Hettangian to Bajocian successions
655 of Dorset and Yorkshire. In: Taylor, P.D. (Ed.), *Field Geology of the British Jurassic*.
656 *Geological Society of London, Bath*, pp. 105–150.

657 Hesselbo, S.P., Pieńkowski, G., 2011. Stepwise atmospheric carbon-isotope excursion during
658 the Toarcian Oceanic Anoxic Event (Early Jurassic, Polish Basin). *Earth Planet. Sci.*
659 *Lett.* 301, 365–372.

660 Hesselbo, S.P., Gröcke, D.R., Jenkyns, H.C., Bjerrum, C.J., Farrimond, P., Morgans Bell, H.
661 S., Green, O.R., 2000. Massive dissociation of gas hydrate during a Jurassic oceanic
662 anoxic event. *Nature* 406, 392–395.

663 Hesselbo, S.P., Jenkyns, H.C., Duarte L.V., Oliveira, L.C.V., 2007. Carbon-isotope record of
664 the Early Jurassic (Toarcian) Oceanic Anoxic Event from fossil wood and marine
665 carbonate (Lusitanian Basin, Portugal). *Earth Planet. Sci. Lett.* 253, 455–470.

666 Howarth, A.S., 1985. Lithostratigraphy of the Staithes Sandstone and Clevand Ironstone
667 formations (Lower Jurassic) of north-east Yorkshire, P. *Yorks. Geol. Soc.*, 45, 261-275.

668 Jenkyns, H.C., 1988. The early Toarcian (Jurassic) event: stratigraphy, sedimentary, and
669 geochemical evidence. *Am. J. Sci.* 288, 101–151.

670 Jenkyns, H.C., 2010. Geochemistry of Oceanic Anoxic Events. *Geochem. Geophys. Geosyst.*
671 11. doi:10.1029/2009GC002788.

672 Jourdan, F., Féraud, G., Bertrand, H., Watkeys, M.K., Renne, P.R., 2008. The $^{40}\text{Ar}/^{39}\text{Ar}$ ages
673 of the sill complex of the Karoo large igneous province: Implications for the

674 Pliensbachian-Toarcian climate change. *Geochem. Geophys. Geosyst.* 9, Q06009,
675 doi:10.1029/2008GC001994.

676 Kafousia, N., Karakitsios, V., Jenkyns, H.C., Mattioli, E., 2011. A Global event with a
677 regional character: the Early Toarcian Oceanic Anoxic Event in the Pindos Ocean
678 (Northern Peloponnese, Greece). *Geological Magazine* 148, 619–631.

679 Kaplan, M.E., 1978. Calcite pseudomorphoses from the Jurassic and lower Cretaceous
680 deposits of northern East Siberia. *Soviet geol. geophys.* 12, 62–70.

681 Kemp, D.B., Coe, A.L., Cohen, A.S., Schwark, L., 2005. Astronomical pacing of methane
682 release in the Early Jurassic period. *Nature* 437, 396–399, doi:10.1038/nature04037.

683 Kontorovich, A.E., Moskvina, V.I., Bostrikov, O.I., Danilova, V.P., Fomin, A.N., Fomichev,
684 A.S., Kostyreva, E.A., Melenevsky, V.N., 1997. Main oil source formations of the West
685 Siberian Basin, *Petroleum Geoscience* 3, 343–358.

686 Knyazev, V.G., Devyatov, V.P., Kutugin, R.V., Nikitenko, B.L., Schurygin, B.N., 2003. Zonal
687 Standard of the Toarcian Stage of the North-East Part of Asia: Resp. red. S.P.
688 Ermakova. - Yakutsk. YB of the SD RAS Publishing House.

689 Küspert, W., 1982. Environmental change during oil shale deposition as deduced from stable
690 isotope ratios, in: Einsele, S., Seilacher A., (Eds.), *Cyclic and Event Stratification*.
691 Springer, New York, pp. 482–501.

692 Léonide, P., Floquet, M., Durllet, C., Baudin, F., Pittet, B., Lécuyer, C., in press. Drowning of
693 a carbonate platform as a precursor stage of the Early Toarcian global anoxic event
694 (Southern Provence sub-Basin, South-east France). *Sedimentology*, DOI:
695 10.1111/j.1365-3091.2010.01221.x.

696 Macchioni, F., 2002. Myths and legends in the correlation between the Boreal and Tethyan
697 Realms. Implications on the dating of the Early Toarcian mass extinction and the
698 Oceanic Anoxic Event. *Geobios Mém. Spec.* 35, 150–164.

699 Mailliot, S., Mattioli, E., Guex, J., Pittet, B., 2006. The Early Toarcian anoxia, a synchronous
700 event in the Western Tethys? An approach by quantitative biochronology (Unitary
701 Associations), applied on calcareous nannofossils. *Palaeogeogr. Palaeoclimatol.*
702 *Palaeoecol.* 240, 562–586.

703 Mattioli, E., Pittet, B., Bucefalo Palliani, R., Röhl, H.-J., Schmid-Röhl, A., Morettini, E.,
704 2004. Phytoplankton evidence for timing and correlation of palaeoceanographical
705 changes during the early Toarcian oceanic anoxic event (Early Jurassic). *J. Geol. Soc.*
706 161, 685–693.

707 Marjanac, T., Steel, R.J., 1997. Dunlin Group Sequence Stratigraphy in the Northern North
708 Sea: A Model for Cook Sandstone Deposition. AAPG Bull. 81, 276–292.

709 Mazzini, A., Svensen, H., Leanza, H.A., Corfu, F., Planke, S., 2010. Early Jurassic shale
710 chemostratigraphy and U–Pb ages from the Neuquén Basin (Argentina): Implications
711 for the Toarcian Oceanic Anoxic Event. Earth Planet. Sci. 297, 633–645.

712 McArthur, J.M., Algeo, T.J., van de Schootbrugge, B., Li, Q., Howarth, R.J., 2008. Basinal
713 restriction, black shales, Re-Os dating, and the Early Toarcian (Jurassic) oceanic anoxic
714 event. *Paleoceanography* 23, PA4217.

715 Meyer, K.M., Kump, L.R., 2008. Oceanic euxinia in Earth history: Causes and consequences.
716 *Annu. Rev. Earth Planet. Sci.*, 36, 251–288, doi:10.1146/annurev.
717 earth.36.031207.124256.

718 Nikitenko, B.L., 2008. The Early Jurassic to Aalenian paleobiogeography of the arctic realm:
719 Implication of microbenthos (foraminifers and ostracodes). *Stratigraphy and Geological*
720 *Correlations* 16, 59–80.

721 Nikitenko B.L., 2009. Jurassic Stratigraphy, Palaeobiogeography and Biofacies of Siberia on
722 Microfauna (Foraminifers and Ostracodes), 680 p. ("Nonparel" Publishing House,
723 Novosibirsk).

724 Nikitenko, B.L., Mickey, M.B., 2004. Foraminifera and ostracodes across the Pliensbachian-
725 Toarcian boundary in the Arctic Realm (stratigraphy, paleobiogeography and biofacies).
726 *J. Geol. Soc. Spec. Publ.* 230, 137–174.

727 Parisi, G., Ortega-Huertas, M., Nocchi, M., Palomo, I., Monaco, P., Martinez, F. 1996.
728 Stratigraphy and geochemical anomalies of the early Toarcian oxygen-poor interval in
729 the Umbria–Marche Apennines (Italy). *Geobios*, 29, 469–484.

730 Prauss, M., Ligouis, B., Luterbacher, H., 1991. Organic matter and palynomorphs in the
731 'Posidonienschiefer' (Toarcian, Lower Jurassic) of southern Germany. *J. Geol. Soc.*
732 *Special Publication* 58, 335–351.

733 Revelle, R., 1990. *Sea Level Change*, 234 p (National Academy Press, Studies in Geophysics,
734 Washington DC).

735 Riding, J.B., Fedorova, V.A., Ilyina, V.I., 1999. Jurassic and Lowermost Cretaceous
736 dinoflagellate cyst biostratigraphy of the Russian Platform and Northern Siberia, Russia.
737 *American Association of Stratigraphic Palynologists Foundation Contributions Series*
738 36, 1-184.

- 739 Röhl, H.-J., Schmid-Röhl, A., 2005. Lower Toarcian (Upper Liassic) black shales of the
740 Central European Epicontinental Basin: a sequence stratigraphic case study from the
741 SW German Posidonia Shale (Lower Toarcian). *SEPM Spec. Publ.* 82, 165–189
- 742 Röhl, H.J., Schmid-Röhl, A., Oschmann, W., Frimmel, A., Schwark, L., 2001. The Posidonia
743 Shale (Lower Toarcian) of SW-Germany: an oxygen-depleted ecosystem controlled by
744 sea level and palaeoclimate. *Palaeogeogr. Palaeoclimatol. Palaeoecol.* 165, 27–52.
- 745 Rosales, I., Quesada, S., Robles, S., 2006. Geochemical arguments for identifying second-
746 order sea-level changes in hemipelagic carbonate ramp deposits. *Terra Nova* 18, 233–
747 240.
- 748 Sabatino, N., Neri, R., Bellanca, A., Jenkyns, H.C., Baudin, F., Parisi, G., Masetti, D., 2009.
749 Carbon-isotope records of the Early Jurassic (Toarcian) oceanic anoxic event from the
750 Valdorbia (Umbria–Marche Apennines) and Monte Mangart (Julian Alps) sections:
751 palaeoceanographic and stratigraphic implications. *Sedimentology* 56, 1307–1328.
- 752 Sahagian, D., Pinous, O., Olfieriev, A., Zakharov, V., 1996. Eustatic curve for the Middle
753 Jurassic–Cretaceous based on Russian platform and Siberian stratigraphy: zonal
754 resolution. *AAPG Bull.* 80, 1433–58.
- 755 Schouten, S., Van Kaam-Peters, H.M.E, Rijpstra, W.E.C, Schoell, M., Sinninghe Damste,
756 J.S., 2000. Effects of an Oceanic Anoxic Event on the stable carbon isotopic
757 composition of early Toarcian carbon. *Am. J. Sci.* 300, 1–22.
- 758 Selleck, B.W., Carr, P.F., Jones, B.G., 2007. A review and synthesis of glendonites
759 (pseudomorphs after ikaite) with new data: assessing applicability as recorders of
760 ancient coldwater conditions. *J. Sediment. Res.* 77, 980–991.
- 761 Shurygin, B.N., 2005. Lower and Middle Jurassic Biogeography, Facies and Stratigraphy in
762 Siberia Based on Bivalve Molluscs, 154 p. (Novosibirsk Academic Publishing House
763 "Geo", Novosibirsk).
- 764 Suan, G., Pittet, B., Bour, I., Mattioli, E., Duarte, L.V., Mailliot, S., 2008. Duration of the
765 Early Toarcian carbon isotope excursion deduced from spectral analysis: consequence
766 for its possible causes. *Earth Planet. Sci. Lett.* 267, 666–679.
- 767 Suan, G., Mattioli, E., Pittet, B., Lécuyer, C., Suchéras-Marx, B., Duarte, L.V., Philippe, M.,
768 Reggiani, M.L., Martineau, F., 2010. Secular environmental precursors to Early
769 Toarcian (Jurassic) extreme climate changes. *Earth Planet. Sci. Lett.* 290, 448–458.
- 770 Svensen, H., Planke, S., Chevallier, L., Malthé-Sorensen, A., Corfu, F., Jamtveit, B., 2007.
771 Hydrothermal venting of greenhouse gases triggering Early Jurassic global warming.
772 *Earth Planet. Sci. Lett.* 256, 554–566.

773 Traverse, A., 2007. *Paleopalynology*. Second Edition. 813 p. (Topics in Geobiology 28,
774 Springer, Dordrecht, The Netherlands).

775 Vakhrameev, V.A., 1991. *Jurassic and Cretaceous floras and climates of the Earth*.
776 Cambridge University Press.

777 van Breugel, Y., Baas, M., Schouten, S., Mattioli, E., Sinninghe Damsté, J.S., 2006.
778 Isorenieratane record in black shales from the Paris Basin, France: Constraints on
779 recycling of respired CO₂ as a mechanism for negative carbon isotope shifts during the
780 Toarcian oceanic anoxic event. *Paleoceanography* 21, PA4220, doi :
781 10.1029/2006PA001305.

782 van de Schootbrugge, B., McArthur, J.M., Bailey, T.R., Rosenthal, Y., Wright, J.D., Miller,
783 K.G., 2005. Toarcian oceanic anoxic event: An assessment of global causes using
784 belemnite C isotope records. *Paleoceanography* 20, PA3008,
785 doi:10.1029/2004PA001102.

786 van de Schootbrugge, B., Harazim, D., Sorichter, K., Oschmann, W., Fiebig, J., Püttmann,
787 W., Peinl, M., Zanella, F., Teichert, B.M.A., Hoffmann, Stadnitskaia, J.A., Rosenthal,
788 Y., 2010. The enigmatic ichnofossil *Tisosa siphonalis* and widespread authigenic seep
789 carbonate formation during the Late Pliensbachian in southern France. *Biogeosciences*
790 7, 3123–3138.

791 Wignall, P.B., 1991. Model for transgressive black shales? *Geology* 19, 167–170.

792 Wignall, P.B., Newton, R., 1998. Pyrite framboid diameter as a measure of oxygen deficiency
793 in ancient mudrocks. *Amer. J. Sci.* 298, 537–552.

794 Wignall, P.B., Newton, R.J., Little, C.T.S., 2005. The timing of paleoenvironmental change
795 and cause- and -effect relationships during the Early Jurassic mass extinction in Europe.
796 *Am. J. Sci.* 305, 1014–1032.

797 Wignall, P.B., Bond, D.P.G., Kuwahara, K., Kakuwa, Y., Newton, R.J., Poulton, S.W., 2010.
798 An 80 million year oceanic redox history from Permian to Jurassic pelagic sediments of
799 the Mino-Tamba terrane, SW Japan, and the origin of four mass extinctions. *Global*
800 *Planet. Change* 71, 109–123.

801 Wilkin, R.T., Barnes, H.L., Brantley S.L., 1996. The size distribution of framboidal pyrite in
802 modern sediments: An indicator of redox conditions. *Geochim. Cosmochim. Ac.* 60,
803 3897–3912.

804 Zakharov, V.A., Bogomolov, Y.I., Ilyina, V.I., Konstantinov, A.G., Kurushin, N.I., Lebedeva,
805 N.K., Meledina, S.V., Nikitenko, B.L., Sobolev, E.S., Shurygin, B.N., 1997. *Boreal*

806 Zonal Standard and Biostratigraphy of the Mesozoic of Siberia. *Geologiya i Geofizika*
807 38, 927–956.

808 Zakharov, V.A., Shurygin, B.N., Ilyina, V.I., Nikitenko, B.L., 2006. Pliensbachian–Toarcian
809 Biotic Turnover in North Siberia and the Arctic Region. *Stratigr. Geol. Correl.* 14, 399–
810 417.

811

812 **Figure captions**

813

814 **Fig. 1.** Location and biostratigraphy of the sections studied and localities mentioned in the
815 text. The two left hand panels show the geographical locations. The right hand panel depicts
816 the palaeogeography of the Early Toarcian; this palaeogeographic map was modified from
817 Nikitenko and Mickey (2004). Abbreviations: PR = Polovinnaya River; AB = Anabar Bay;
818 KR = Kelimyar River; WSB= W Siberian Basin.

819

820 **Fig. 2.** Biostratigraphy and lithostratigraphy of the sections studied. A) Biostratigraphy of the
821 Olenek-Kelimyar Rivers area compared to equivalent Boreal and NW European ammonite
822 zones. The relationships between different biostratigraphical schemes of the Olenek-Kelimyar
823 Rivers area have been constructed using new macropalaeontological and
824 micropalaeontological data from several sections in this area (see list and location of these
825 sections in Knyazev et al, 2003). B) biostratigraphy, lithological characteristics and proposed
826 correlation of the Pliensbachian-Toarcian sections studied from N Siberia. The ammonite
827 biostratigraphy of the Kelimyar River section has been refined using the well-constrained
828 foraminifera and dinoflagellate cyst zones of the section and their relationships with
829 ammonite zones in several coeval sections nearby. The foraminifera and dinoflagellate cyst
830 biostratigraphy of the Polovinnaya River section is from this study and that of Anabar Bay
831 section is from Riding et al. (1999) and Knyazev et al. (2003); the bivalve, dinoflagellate cyst
832 and foraminifera zones from these two sections were used to infer tentatively the positions of
833 ammonite zones by comparison with other sections (see text). Abbreviations: *a* = *antiquum*;
834 *falc* = *falciferum*; *com* = *commune*; *braun* = *braunianus*; A-zone = ammonite zone; F-zone =
835 foraminifera zone; D-zone = dinoflagellate cyst zone.

836

837 **Fig. 3.** Evidence for near-freezing conditions in polar regions prior to the T-OAE. A) *In situ*
838 glendonites (arrows) from the Upper Pliensbachian of Anabar Bay; B) Isolated glendonite
839 specimen from the Upper Pliensbachian of Anabar Bay (scale bar=1 cm); C) and D) Thin

840 section of the specimen depicted in B, showing the contact between the stellate margin of the
841 glendonite and the fine-grained matrix; note also the granular texture of the replacive calcite
842 (scale bars=500 μm ; D, crossed nicols); E) and F) An isolated limestone boulder (maximum
843 width= \sim 20 cm) encrusted by *Harpax* bivalves from the Upper Pliensbachian homogenous
844 siltstone at Kelimyar River.

845

846 **Fig. 4.** Total Organic Carbon (TOC), Hydrogen Index, pyrite framboid and organic carbon
847 isotope ($\delta^{13}\text{C}_{\text{TOC}}$ data) for the Pliensbachian and Toarcian strata of N Siberia. Each point of
848 the pyrite framboid profile represents the average size of 30 pyrite framboids and the error
849 bars are 95% confidence intervals. See Fig. 1 for details on the biostratigraphy of the sections
850 studied. *a.* = *antiquum*; *braun.* = *braunianus*; *falc.* = *falciferum*; *com.* = *commune*; A-zone =
851 ammonite zone.

852

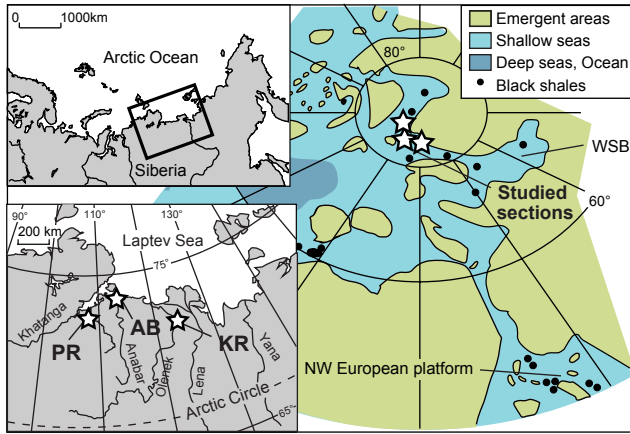
853 **Fig. 5.** Origin of the sedimentary organic matter from the Pliensbachian and Toarcian strata of
854 N Siberia and relationships with its carbon isotopic composition. A) Hydrogen Index (HI)
855 versus T_{max} values and B) versus Oxygen Index (OI) for Polovinnaya River and Kelymiar
856 River samples, illustrating the kerogen types and probable origin of the organic matter; C)
857 Hydrogen index versus $\delta^{13}\text{C}_{\text{TOC}}$ values obtained for Polovinnaya River and Kelymiar River
858 samples; D) TOC versus $\delta^{13}\text{C}_{\text{TOC}}$ values obtained for Anabar Bay, Polovinnaya River and
859 Kelymiar River samples. AB=Anabar Bay; KR= Kelimyar River; PR= Polovinnaya River.
860 TOC =total organic carbon content of the samples analyzed.

861

862 **Fig. 6.** Comparison of climatic, geochemical and biotic records of the T-OAE between polar
863 and tropical latitudes. A) Climatic and biotic events in the Arctic. The level of the mass
864 extinction and main biotic events are from Zakharov et al. (2006); B) Chronostratigraphy,
865 Total Organic Carbon (TOC), Hydrogen Index and organic carbon isotope ($\delta^{13}\text{C}_{\text{TOC}}$) data
866 from Kelimyar River; C) Chronostratigraphy, TOC, Hydrogen Index and $\delta^{13}\text{C}_{\text{TOC}}$ data from
867 Dotternhausen (filled circles) and Zimmern (squares) modified from Küspert (1982), Prauss et
868 al. (1991) and Röhl et al. (2001) and estimated duration of the CIE following Cohen et al.
869 (2007) and Suan et al. (2008); D) Seawater palaeotemperatures derived from the oxygen
870 isotope composition of belemnites from Dera et al. (2009) and the mass extinction level at
871 low-latitudes from Caswell et al. (2009). *a.* = *antiquum*; *bifr.* = *bifrons*; *braun.* = *braunianus*;
872 *ten.* = *tenuicostatum*; *v.* = *variabilis*; U.T. = Upper Toarcian; A-zone = ammonite zone.

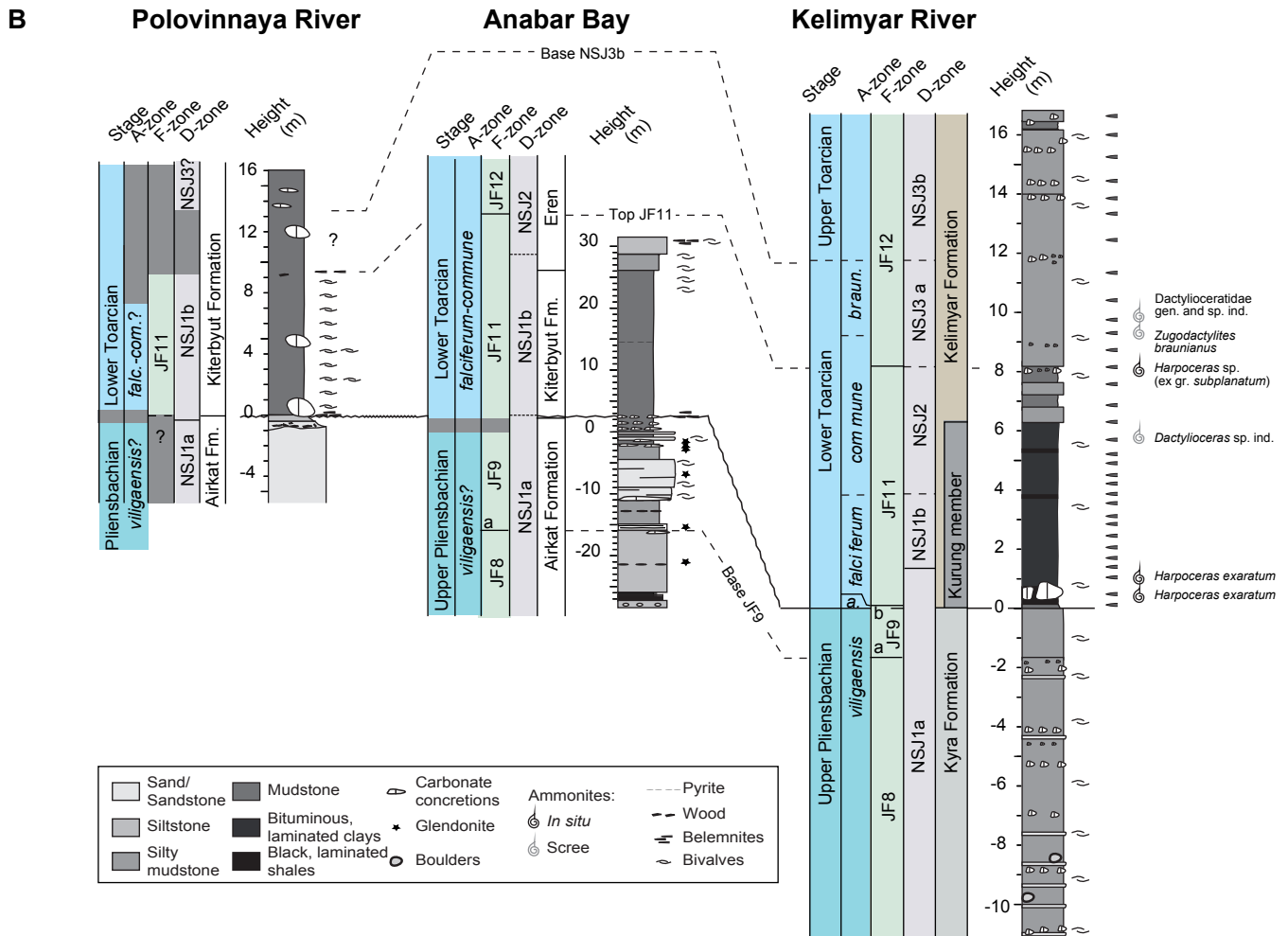
873

874 **Fig. 7.** Organic carbon isotope ($\delta^{13}\text{C}_{\text{TOC}}$) and Total Organic Carbon (TOC) trends in polar and
875 tropical areas during the Pliensbachian–Toarcian interval. A) Shallow water section of
876 Anabar Bay, N Siberia; B) Deep shelf record of Kelimyar River, N Siberia; C) Deep water
877 record of Dotternhausen and Zimmern, SW Germany (modified from Küspert, 1982, Prauss et
878 al., 1991 and Röhl et al., 2001); D) Shallow water record of NE France (modified from van
879 Breugel et al., 2006); E) Open-ocean record of Valdorbia, central Italy (isotope and TOC data
880 modified from Sabatino et al., 2009; Biostratigraphy from Bilotta et al., 2010). *a.* = *antiquum*;
881 *bifr.* = *bifrons*; *braun.* = *braunianus*; *mir.* = *mirabilis*; *serp.* = *serpentinus*; *ten.* =
882 *tenuicostatum*; U.T. = Upper Toarcian; A-zone = ammonite zone; N-zone, nannofossil zone.
883



Suan et al., Fig. 1

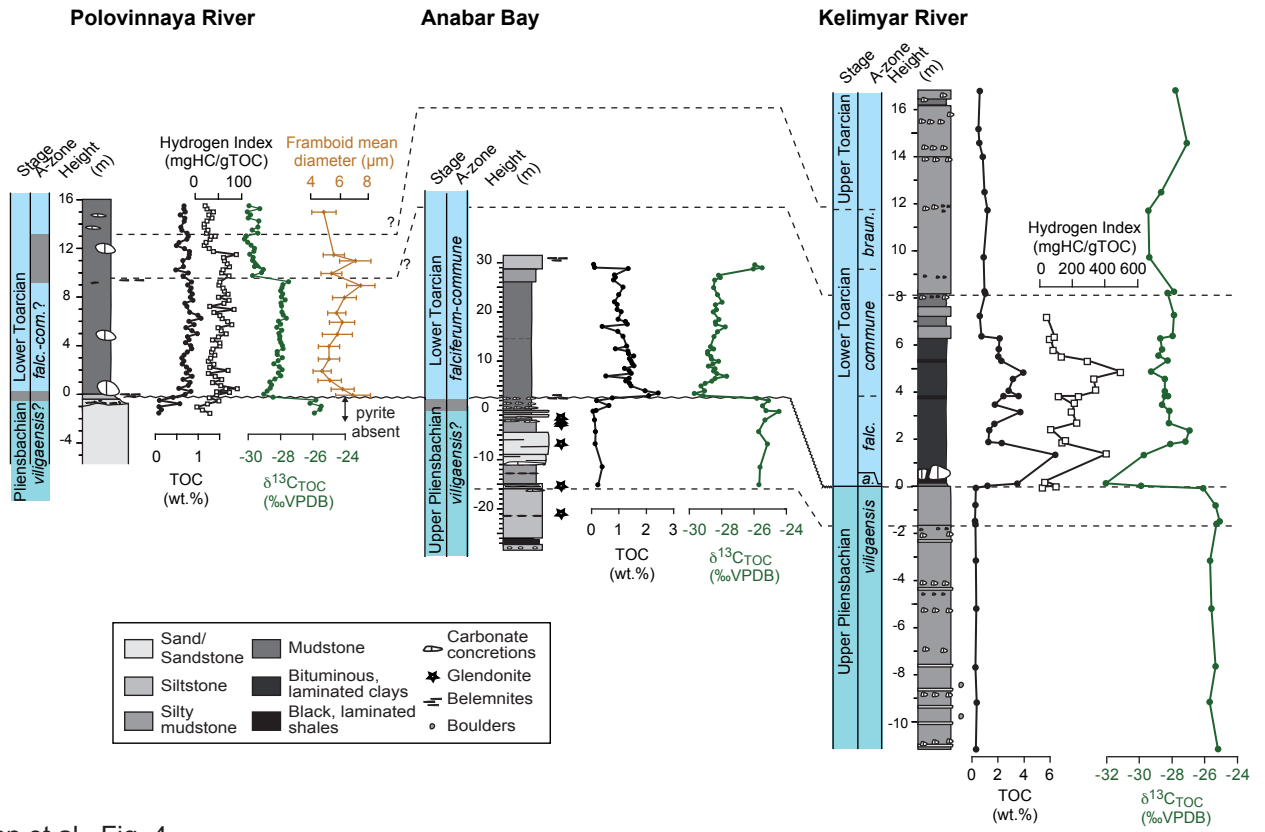
Stage	Sub-stage	NW European ammonite zones	Boreal ammonite zones	Biostratigraphy of the Olenek and Kelimyar Rivers area			Lithostratigraphy			
				Ammonites	Foraminifera	Dinoflagellate cysts	AB & PR	Olenek & KR		
Toarcian	Upper	<i>P. dispensum</i>	<i>Pseudolioceras falcodiscus</i>	?	<i>Astacolus praefoliaceus</i> , <i>Lerticulina multa</i>	<i>Trochamina taimyrensis</i>	NSJ3 <i>V. aquilonum</i> , <i>N. triangulata</i>	Khorgo Fm ~15–30 m	Kelimyar Fm (lower part)	
		<i>G. thouarsense</i>	<i>Pseudolioceras wuerttenbergi</i>	<i>P. wuerttenbergi</i>				NSJ3b NSJ3a <i>P. eumekes</i>		Eren Fm
		<i>Haugia variabilis</i>	<i>Pseudolioceras compactile</i>	<i>P. compactile</i>						NSJ2 NSJ1b NSJ1a <i>Nannoceratopsis gracilis</i> <i>N. deflandrei senex</i> <i>N. deflandrei anabarensis</i>
	Lower	<i>Hildoceras bifrons</i>	<i>Porpoceras spinatum</i>	<i>Zugodactylites monestieri</i>	<i>Zugodact. braunianus</i>	JF13 <i>Trochamina kisseimani</i>	NSJ1 <i>Nannoceratopsis deflandrei</i>	Kiterbyut Fm ~24–28 m		
			<i>Dactylioceras commune</i>	<i>D. commune</i>	<i>Ammobaculites lobus</i> , <i>Trochamina kisseimani</i>	JF12 <i>Trochamina kisseimani</i>				
		<i>H. serpentinum</i> (= <i>H. falciferum</i>)	<i>H. falciferum</i>	<i>H. falciferum</i>	<i>H. falciferum</i>	<i>Recurvoides taimyrensis</i>	JF11 <i>Trochamina kisseimani</i>	JF9		Upper Mbr
<i>D. tenuicostatum</i>	<i>T. antiquum</i>	<i>Amaltheus sp.</i> (ex gr. <i>viligaensis</i>)	<i>Conoroides bulimoides</i>	<i>Anmarginulina artica</i>	JF8	JF7	Airkat Fm ~35–70 m			
Pliensbachian	Upper	<i>Pleuroceras spinatum</i>	<i>Amaltheus viligaensis</i>	<i>Amaltheus margaritatus</i>	<i>Anmarginulina gerkei</i>	JF6	JF5	Lower Mbr ~40–80 m	Kyra Fm (upper part) ~50 m	
		<i>Amaltheus margaritatus</i>	<i>Amaltheus margaritatus</i>	<i>Amaltheus stokesi</i>	<i>Trochamina lapidosa</i> , <i>Fronidulinita dubiella</i>	JF4	JF4			
		<i>Amaltheus stokesi</i>	<i>Amaltheus stokesi</i>							



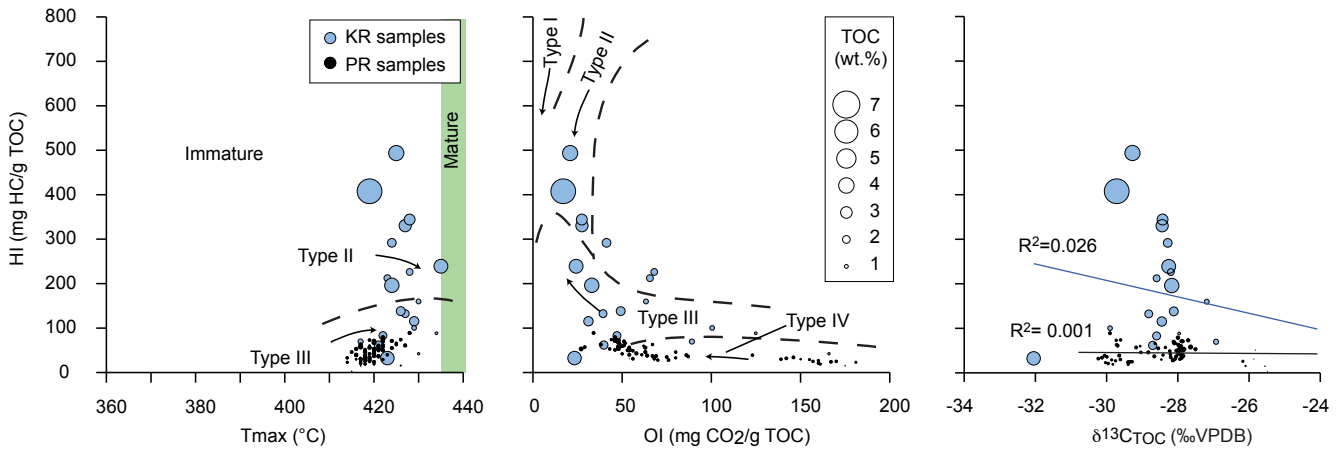
Suan et al., Fig. 2



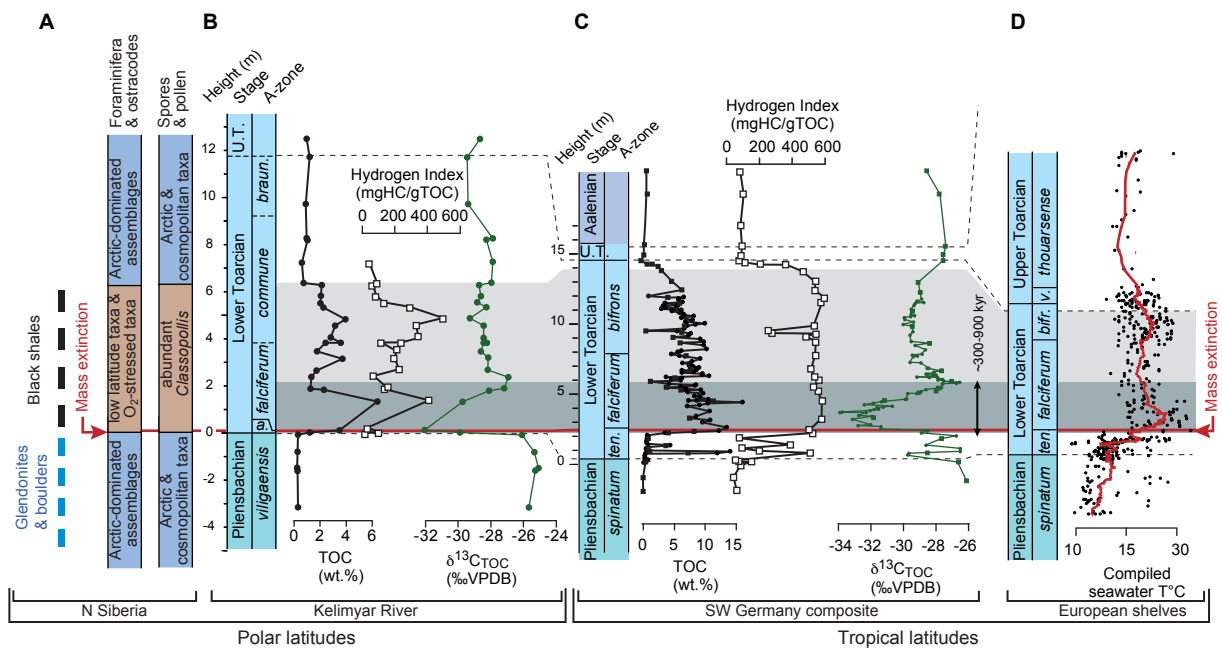
Suan et al., Fig. 3



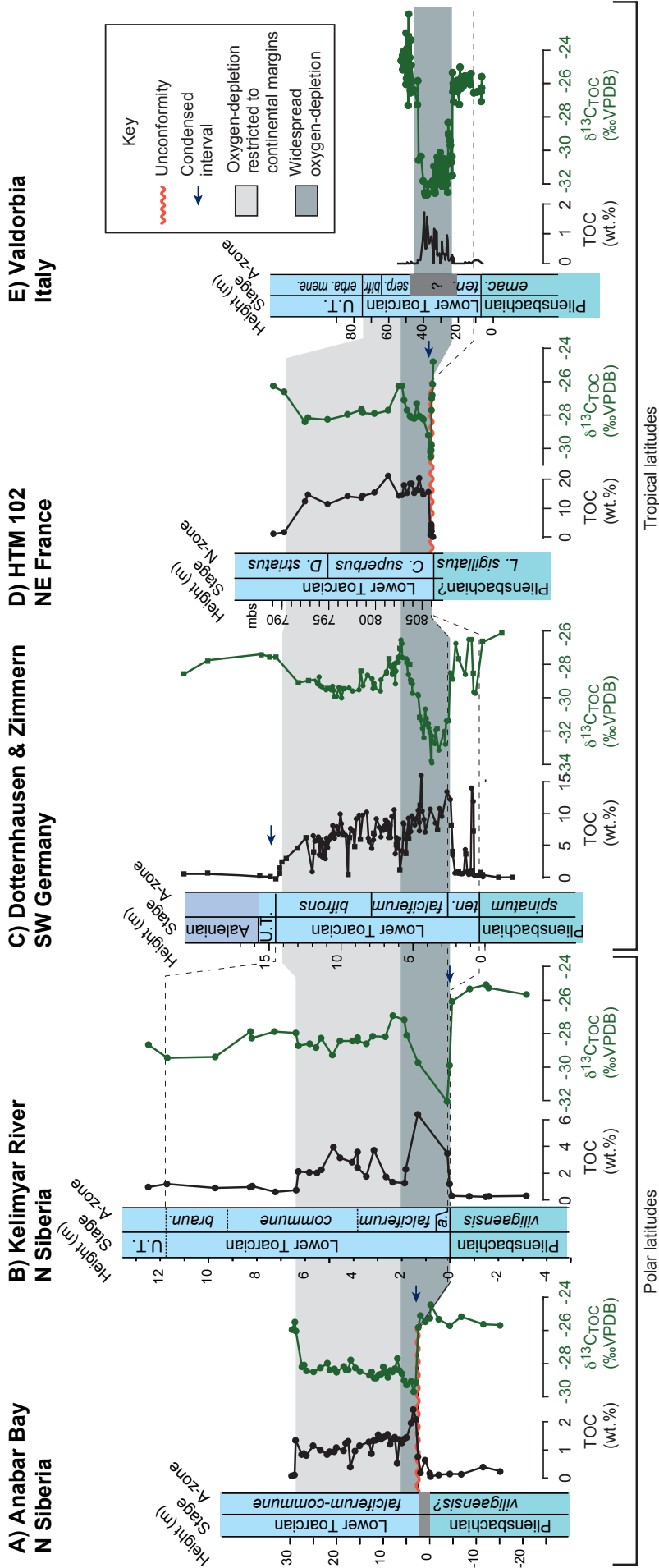
Suan et al., Fig. 4



Suan et al., Fig. 5



Suan et al., Fig. 6



Suan et al., Fig. 7